A Novel Approach for Colon Biopsy Image Segmentation

Saima Rathore

Department of Computer and Information Sciences
Pakistan Institute of Engineering and Applied Sciences,
Islamabad, Pakistan

saimarathore_2k6@yahoo.com

Mutawarra Hussain, Asifullah Khan

Department of Computer and Information Sciences
Pakistan Institute of Engineering and Applied Sciences,
Islamabad, Pakistan

{mutawarra, asif } @pieas.edu.pk

Abstract— Colon cancer is one of the leading causes of deaths worldwide. Traditionally, colon cancer is diagnosed using microscopic analysis of colon biopsy images. However, computer based diagnosis involves acquiring a biopsy image, segmenting the image into constituent regions, extracting features, and based on features identifying cancerous and non-cancerous regions. Image segmentation that is the core process in overall diagnosis is extremely challenging due to similar color distribution in various biological regions of histopathological images. Problem gets more complicated for homogenous images or images acquired under different conditions, particularly change in magnification factor. Several segmentation schemes, proposed for colon images, do not address these problems. In this research study, we propose an un-supervised colon biopsy image segmentation scheme that incorporates background knowledge of benign and malignant tissue organization. The scheme detects elliptical epithelial cells in four angular directions of 0°, 45°, 90°, 135°, and divides elliptic constituents into distinct 'primitives. It further makes use of the distribution as well as spatial relations of these 'primitives' to define a homogeneity measure for identifying regions. Contrary to previous ones, the proposed scheme removes dependency on change in magnification and image type. Genetic algorithm (GA) has been employed to optimize several system parameters such as semi-major and semi-minor axis of ellipse, component area threshold to remove smaller components, and merge factor to merge two adjacent and similar regions. Algorithm has been tested on 100 colon biopsy images and improved segmentation accuracy has been observed when compared with segmentation results obtained using circular primitive based techniques.

Index Terms - Colon cancer, Segmentation, Elliptic primitives, Colon biopsy

I. INTRODUCTION

Colon is one major constituent of large intestine. Its cancer causes deaths of about half a million people each year. Major reasons of colon cancer are diets low in fruit and vegetation, and high in fat, excessive smoking and increasing age. Cancer is caused by abnormal growth of tissue and turning into colonic polyps. Polyps are usually benign, and show cancer symptoms after 5-6 years of their startup by the time cancer is too late to cure. Traditionally, colon cancer is diagnosed using microscopic analysis of histopathological tissue samples. Pathologists assign cancer grades to the samples depending upon the deformation of cells they observe in images. Usually, five stages of colon cancer, 0, A-D, are assigned using Duke's scale [1, 2]. 0 is the starting stage in which cancer has just started to develop and tissues are still coherent, whereas D is the final cancer stage in which cancer has reached other body parts such as lungs. In stage D, colon tissues are poorly deformed, unstructured and have almost amorphous shape.

Microscopic inspection of biopsy samples is time-consuming and laborious task for the histopathologists, and leads to significant inter-observer variation in grading [3, 4]. Heterogeneity of features in some regions also adds to the delicacy of diagnosis. Such problems become critical if the results of the biopsy sample are to be used for deciding treatment plans; therefore, automatic techniques are mandatory. Automation of microscopic analysis would be of great help to pathologists, as they have many images to assess in routine.

Researchers have proposed several automatic colon cancer detection schemes, which vary in terms of algorithm, equipment and dataset however they all share common goal of high classification rates with the reduced need of subjective involvement of trained histopathologists. A subset of these schemes performs hyperspectral analysis on colon biopsy images and classifies samples into benign and malignant classes [5-8]. Another interesting and quite promising method of colon cancer detection is simultaneous analysis of thousands of human genes [9-10]. Such schemes study genetic alterations in stomatic cells caused by colon cancer using two variants of microarrays. Texture of colon tissues is also focus of few studies. Some researchers have exploited the noteworthy contrast between texture of cancerous and non-cancerous parts of colon biopsy images, and have used textural features of cytological tissue components to demarcate benign and malignant image constituents [11-13]. Laser-induced fluorescence and Raman spectroscopy of serum has also been used in few studies [14-20]. Researchers have exploited the variation in chemical composition and resulting raman spectra of normal and cancerous blood serum for cancer diagnosis. A new fascinating way of cancer detection is to analyze colon images, and to measure the degree of coherence and well-defined organizational structure of the perceived picture [21, 22]. Automatic techniques definitely improve performance and cut down medical resources otherwise necessary. However, they still have not been used as decisive bodies and manual processing by a clinical expert remains the gold standard against which results are compared.

Relatively little effort has been expended on colon tissue segmentation. Most of the schemes, discussed previously, focus on direct classification of colon tissues while skipping intermediate segmentation. Segmentation of colon biopsy images is extremely hard. Color intensities are almost similar in both the cancerous and non-cancerous portions of the image, thus making intensity based segmentation almost impossible. Only known solution is to incorporate knowledge about organization of normal and malignant colon tissues into the segmentation process. There are a few such schemes, known as object oriented texture analysis techniques [23-26], which do so. OSEG [23] and GRLM [24] are the major representatives

of this category. Initially, both the schemes extract circular primitives from image, but in later stages, OSEG makes use of spatial arrangement and size of primitives for region identification, whereas GRLM calculates graph run-length matrices of primitives for identifying regions. But the problem with such schemes is that they perform well on the type of image for which they are programmed, like, OSEG and GRLM are highly tuned on biopsy images, taken at 5x magnification, and could segment only heterogeneous images. These schemes produce inappropriate results if tested on homogenous images or images taken at any other microscopic magnification. Reason behind failure is elliptic contour of epithelial cells; they seem circular at a smaller magnification of 5x, but as magnification increases, their elliptic shape gets prominent. Both the schemes assume epithelial cells as circular and extract largest possible circular primitive from the elliptic shape. Many pixels, which are actually part of the primitive, are not marked as its constituents, thus ultimately resulting in lower accuracy. Moreover, these schemes require adjustment of several system variables on hit and trial basis.

In this paper, we propose an improved version of colon biopsy image segmentation scheme, and call it Modified Object based Segmentation (MOSEG). Our segmentation scheme though captures basic idea from [23], exploits spatial distribution and size of cytological tissue components in an entirely different fashion. First, in object identification process, elliptic primitives are found in four angular directions to extract as many epithelial cells as possible. Second, a membership function has been introduced to reduce the effect of noise, and to help in detecting larger number of primitives. Use of elliptic shapes instead of circular ones greatly increases number of primitives, which are detected, and hence the number of pixels, assigned to primitives. Third, GA has been employed to get rid of manual adjustment of system parameters, and automatically find optimal values for these parameters at all magnification factors. These automations make our scheme independent of magnification factor and image type.

Remaining paper is organized as follows. Section 2 describes proposed scheme in detail. Section 3 demonstrates experimental results whereas Section 4 concludes the paper.

II. PROPOSED SCHEME

Overall scheme, represented in Fig. 1, can be categorized into two distinct phases; 1) image segmentation, and 2) GA based parameter optimization. Image segmentation is the core module that needs automatic adjustment of a few parameters. GA is used to find optimal values of these parameters. GA based parameter optimization process is repeated four times, individually for different magnification factors. Once optimal values are achieved, they are used in segmentation of test data.

Segmentation process comprises following major phases: 1) image acquisition, 2) clustering, 3) primitive identification, 4) primitive categorization, 5) feature extraction, 6) initial seeds identification, 7) seed growing, and finally 8) region merging. Fig. 2 portrays top-level layout of the segmentation process, however, following text elaborates these phases in detail.
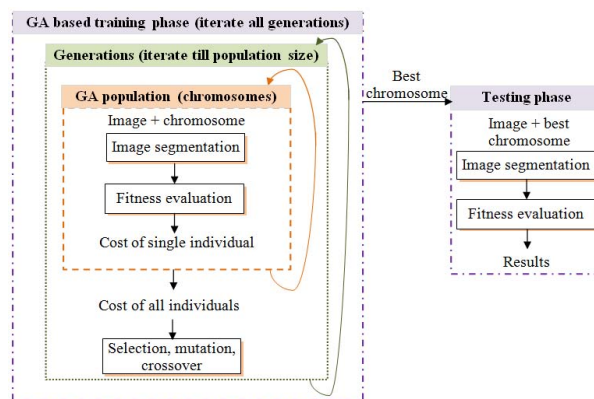

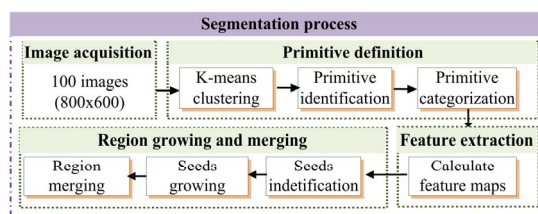Figure 1. Top level layout of proposed scheme

Figure 2. Top level layout of segmentation process

A. Image Acquisition

Our experimental dataset consists of 100 biopsy samples, taken from 100 randomly selected patients from the pathology department archives of Rawalpindi Medical College. Biopsy samples, comprising of 5–6 μm thick tissues, are stained with Hematoxylin & Eosin. Nikon Biophot microscope is used with four different magnification factors for capturing RGB images.

B. Primitive Identification

Previous techniques [23, 24] search epithelial cells as circular primitives in biopsy images. However, in real biopsy images, epithelial cells are not circular rather they are elliptical. Previous techniques, when fit circular primitives in these elliptical cells, many pixels that lie outside the boundary of the detected circle are not assigned to the primitive. This phenomenon results in lower accuracy especially at higher magnification factors. In order to alleviate such problems, we have introduced a new primitive extraction mechanism presented in Fig. 3.
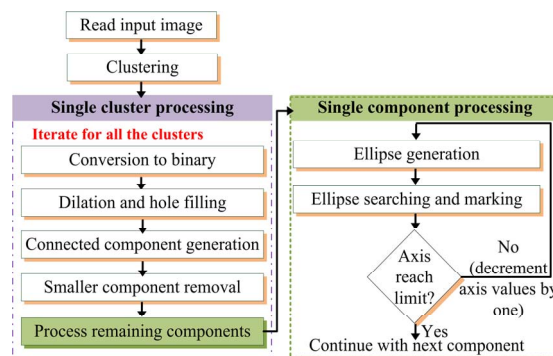

Figure 3. Ellipse extraction algorithm

K-means is applied to divide image pixels into clusters of pink colored connective components, white colored luminal

structures, and purple colored epithelial cells and lymphoid cell components. Clusters are converted to binary mode, dilation and hole filling are performed to make the clusters suitable for finding ellipses. Connected components are found in each cluster, and components having area smaller than Component Area Threshold (CAT) are removed. Optimal value of CAT is found through GA. Four simulated ellipses, as given in Fig. 4, are then generated starting with maximum values of semi-major axis (MAL) and semi-minor axis (mAL).
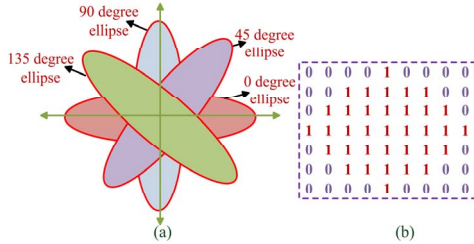

Figure 4.   (a) Four angular ellipses (b) Horizontal ellipse (MAL=4, mAL = 3)

MAL is optimized through GA, whereas mAL is always kept 2 units smaller than MAL. Suppose MAL is 4 pixels and mAL is 3 pixels long, then horizontal, vertical, and diagonal ellipses are matrices of size 7x9, 9x7 and 9x9 respectively. Pixels lying inside ellipse have value '1', whereas outer pixels have value '0' as demonstrated in Fig. 4 (b). System searches as many ellipses as possible in each component. In case ellipses are found, corresponding pixels are marked with a unique primitive identifier. Axes values are decremented by one unit; ellipses with new values are generated again and found in the component. Process is continued with remaining pixels which are not assigned to any elliptic primitive until axes values reach their lowest possible value. Ellipse finding itself is a pattern matching process. It traverses pixels of component one by one, and extracts window, around given pixel, of same size as ellipse. Extracted window is matched against given ellipse pixel by pixel basis. If all the pixels having value '1' in ellipse are also '1' in window, there is ellipse at central pixel.

There may be some cases, where due to blur or noise, some pixels of elliptic components may be 0, resulting in not exact but nearly elliptic shapes in the image. In order to impart capability of finding such nearly elliptic shapes, we have introduced a membership function which defines percentage of pixels that should strictly be same in ellipse and extracted window. Membership value is 95% in our case. A side advantage of finding ellipses in different directions is alleviation of the problem of biopsy slide and tissue orientation on microscope. Likewise, introduction of ellipse instead of circular primitives greatly increases number of detected primitives and pixels, and hence improves segmentation accuracy. Fig. 5 demonstrates the difference.
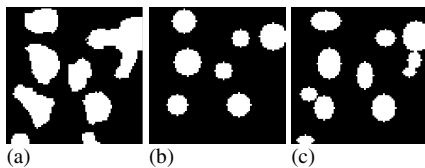

Figure 5.   (a) Cluster, primitives using (b)circular, and (c) elliptic shapes

Fig. 5(a) represents a cluster of size 80x80 (1600 pixels) only. Pixels spanned by circles (given in Fig. 5(b)) and ellipses (given in Fig. 5(c)) are 966 and 1345 respectively. Four maps are maintained for each cluster to store information about its primitives. A 'Primitive Map' stores pixels that belong to primitives. Similarly, 'Semi-major Axis', 'Semi-minor Axis' and 'Direction' maps are maintained to store values of semi-major axis, semi-minor axis and orientation of the identified primitive at respective center locations.

C. Primitive Categorization

Primitives of each cluster are further divided into two categories/types depending upon certain Primitive Area Threshold (PAT), thus giving a total of six circular object types, two for each cluster. Primitives divide into category 1 and 2 for cluster 1, category 3 and 4 for cluster 2, and finally category 5 and 6 for cluster 3. By size we mean number of image pixels primitive spans. A 'Primitive' map is maintained that stores category of each primitive at respective center locations. PAT is a user-defined parameter that is also optimized through GA.

D. Feature Extraction

Feature extraction phase computes twelve uniformity measures, similar to the ones used in [23]. For this purpose, a circular window is placed at each image pixel and two uniformity measures are computed for each of six primitive categories, thus giving a total of twelve uniformity measures for each individual pixel. Two uniformity measures include: 1) Primitive Size Uniformity (PSU) and 2) Primitive Spatial Distribution Uniformity (PSDU). PSU measures co-efficient of standard deviation for each particular primitive type lying within a circular window around given pixel, whereas PSDU is calculated using magnitude of sum of position vectors for each particular primitive type lying within a circular window around given pixel. Position vectors are calculated with reference to the centre of circular window.

Values for these primitives approach to zero in case primitives have uniform size or they are uniformly distributed in given window. Features are computed using smaller and larger circular window in order to capture local as well as global textural information. Calculation of radii for both windows depend upon the size of largest primitive, found in image, and is given in Equation (1).

$$LargeWinRad = \max(\max(MajorAxis)), SmallWinRad = LargeWinRad - 5 \quad --(1)$$

Twelve feature maps are maintained to store features for individual pixels.

E. Initial Seed Identification

In this phase, pixels having values of all uniformity measures less than corresponding threshold are marked as seeds. Threshold is calculated separately for each uniformity measure by adding corresponding mean and standard deviation value over all pixels. Seeds, obtained using larger and smaller windows, are merged together. Merged seeds, which have size smaller than smaller window, are eradicated.

F. Seed Growing

In seed growing, threshold values are re-computed using remaining pixels. Pixels with values of measures less than updated threshold are added to make new connected components. There are three possible options for the new component: it is (1) declared new seed if it has no adjacent neighbor, (2) merged to the neighbor in case it has only one

neighbor, (3) merged to the closest (adjacent and similar) neighbor in case it has more than one neighbor.

In successive iterations, only remaining pixels which do not belong to any region participate in threshold computation. Value of standard deviation has been increased by 20% in subsequent iterations to reduce computation burden and to merge maximum possible pixels to the regions.

G. Region Merging

Region merging phase, typically used to avoid over-segmentation, is based on two features: percentage of total area of each primitive type in a region, and percentage of combined areas of different primitives that belong to particular cluster type in the region. Two regions are merged if they are adjacent, and Euclidean distance between their features is less than merge threshold. Merge threshold is computed as average Euclidean distance amongst features of regions. A Merge Factor (MF) has also been introduced to increase/decrease the value of merge threshold. It is also optimized through GA.

H. Genetic Algorithm based Parameter Optimization

GA strives to maximize/minimize an objective function by simulating natural evolution and using genetic operators. GA starts with an initial random population of individuals spanning entire search space. Individuals are combinations of random values for system parameters. Individuals are evolved and genetic operators are applied on them in successive generations. Fit individuals pass on next iteration whereas unfit ones die. Process continues until individuals converge to an optimal solution. Such a combination of diverse population, natural evolution and genetic operators makes GA most suitable tool to find optimal parameter values. We have obtained optimal values of four parameters, namely, MF, MAL, PAT and CAT through GA. PAT, CAT and MAL, all are measured in number of pixels.

III. EXPERIMENTAL RESULTS

100 RGB images of colon biopsies and relevant expert opinion have been used in experiments. Homogenous and heterogeneous images are captured at four different magnification factors of microscope i.e. 4x, 5x, 10x and 40x. Each image has a spatial resolution of 800x600. Images are homogeneous, comprising cancerous/non-cancerous tissues, as well as heterogeneous, comprising both tissue types. Statistics for data are given in Table I.

TABLE I.   DATA SET STATISTICS

Magnification factor	4x	5x	10x	40x	Total
No. of homogeneous images	05	08	07	05	**25**
No. of heterogeneous images	20	20	28	07	**75**
Total	**25**	**28**	**35**	**12**	**100**

Three types of experiments were conducted individually on the given dataset. In the first two experiments, OSEG and GRLM techniques were tested using our dataset. Several parameters were manually adjusted for OSEG and GRLM which are given in Table II.

TABLE II.   PARAMETERS SETTING FOR OSEG AND GRLM

Parameter name	Parameter value
Minimum circle radius	2 pixels
Component area threshold	100 pixels
Merge threshold	1.2
Smaller and larger window sizes	96 pixels and 253 pixels
Size and type of structuring element	2 , Disk

In the third experiment, GA was run individually on images of different magnification factors to find optimal parameter values, while maximizing segmentation accuracy. In each of four scenarios, GA was run with initial random population and for maximum of 200 iterations. Values of GA variables, and range of values for different system parameters are given in Table III. GA searches for optimal values of system parameters within given ranges.

TABLE III.   GA PARAMETERS AND RANGES FOR SYSTEM PARAMETERS

Values of GA variables			
GA Variable	*Value*	*GA Variable*	*Value*
Initial population size	30	Cross-over rate	0.8
Population type	Random	Fitness function	Accuracy
Mutation rate	Default	No. of iterations	200
Ranges defined for system parameters			
System parameter	*Range*	*System parameter*	*Range*
MF	0-5	CAT	10-100
MAL	05-100	PAT	10-500

GA was run with settings given in Table III and optimal values of system parameters for various magnification factors were obtained. Optimal parameter values and number of iterations elapsed before convergence of GA are given in Table IV.

TABLE IV.   OPTIMAL VALUES FOR SYSTEM PARAMETERS CALCULATED BY GA AT DIFFERENT MICROSCOPIC MAGNIFICATION, AND GA ITERATIONS

	4x	5x	10x	40x
MF	1.2	1.0	0.8	0.6
MAL	08	11	20	55
CAT	27	25	37	46
PAT	63	98	209	364
Number of Iterations	88	97	163	132

Table IV reveals that number of iterations do not follow any regular pattern and hence are independent of magnification factor. However, parameter values show clear diversity with increasing magnification factor from left to right. Increase in magnification factor decreases visible biopsy area and increases details within the area. It produces a zoom in effect in the image, visible primitives and connected components get enlarged, whereas number of visible primitives gets reduced. As primitives become enlarged, optimal length of semi-major axis to find them, and optimal PAT value to categorize primitives increases. Optimal value of CAT does not show significant increase and maintains almost steady value, because what so ever the magnification is, it is always good to remove smaller number of components having smaller area. Optimal value of MF decreases because with increasing magnification, heterogeneous regions become more prominent, and hence lesser number of regions gets merged. Once optimal values are achieved, MOSEG is evaluated on given dataset.

In all the experiments, number of primitives detected by different schemes, and percentage of image pixels occupied by

the primitives were noted. Fig. 6 and Fig. 7 show comparison between these two factors for different schemes, where one can see a notable increase in both the factors in case of MOSEG when compared against OSEG and GRLM.
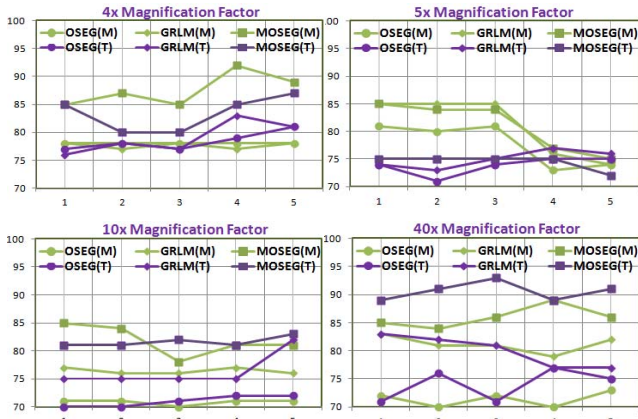

Figure 6.   Pixels(percentage) comparison of OSEG, GRLM and MOSEG
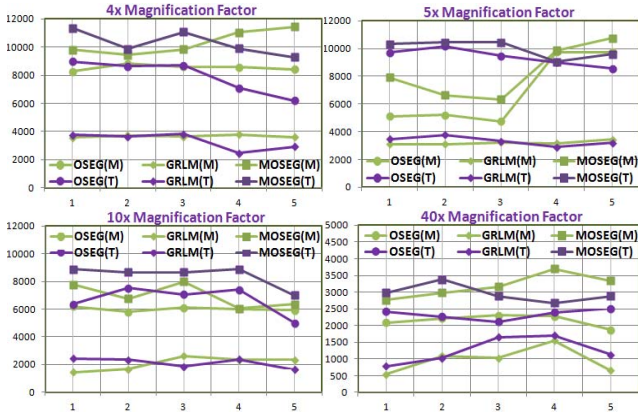

Figure 7.   Primitive comparison of OSEG, GRLM and MOSEG

Fig. 6 and Fig. 7, respectively, show comparison of pixels and primitives, calculated for images of different magnification factor by different schemes. 'Purple' and 'Green' color lines represent Heterogeneous and Homogenous images (represented by T and M in the legend entry) respectively. Legend types represent individual schemes such as 'Square', 'Circle' and 'Diamond' legends represent MOSEG, OSEG and GRLM respectively. Close analysis reveals that at 4x, 10x and 40x magnification factors, our scheme detects more primitives and marks greater percentage of image pixels as compared to other schemes. However, in case of 5x magnification factor, OSEG and GRLM detect almost same primitives and percentage of image pixels as our scheme does. Primary reason is that both these schemes are inherently designed for 5x magnification and epithelial cells possess almost circular shape at this magnification factor.

Visual segmentation results for OSEG, GRLM and MOSEG are given in Fig. 8 (a1-a2), Fig. 8 (b1-b2) and Fig. 8 (c1-c2), respectively. Segmentation results demonstrate clear supremacy of MOSEG over others. MOSEG divided first image into three regions (Fig. 8 (c1)), whereas GRLM missed the top-right region in Fig. 8 (b1) and divided image into two regions. OSEG merged bottom central area with middle area

and also segregated image into two regions in Fig. 8 (a1). Similarly, MOSEG captured heterogeneity very well and divided image into four regions in Fig. 8 (c2). However, both OSEG and GRLM could not distinguish top-left region and partitioned image into two regions only.

We have used Sensitivity (*Sen*), Specificity (*Spe*) and Accuracy (*Acc*) to compare MOSEG against OSEG and GRLM. In order to calculate these parameters, segmented binary images are compared against ground truth binary images and number of true positives (TP), true negatives (TN), false positive (FP) and false negative (FN) are calculated. Corresponding performance measures are given in Table V.

$$Sen = \frac{TP}{TP+FN}, Spe = \frac{TN}{TN+FP}, Acc = \frac{TN+TP}{TN+TP+FN+FP}$$

TABLE V.   PERFROMANCE COMPARISON OF OSEG, GRLM AND MOSEG

		OSEG			GRLM			MOSEG		
		Sen	*Spe*	*Acc*	*Sen*	*Spe*	*Acc*	*Sen*	*Spe*	*Acc*
4x	M	75.41	54.37	**59.31**	66.93	71.65	**62.30**	90.76	88.43	**74.87**
	T	88.45	50.29	**60.53**	92.59	60.25	**65.58**	88.54	76.59	**76.99**
5x	M	76.30	56.18	**62.21**	86.34	67.19	**68.75**	93.87	83.65	**80.55**
	T	94.19	73.42	**81.29**	93.38	80.45	**83.50**	88.56	85.43	**85.77**
10x	M	87.19	43.76	**60.05**	70.36	50.68	**61.58**	90.65	86.66	**88.98**
	T	84.60	41.68	**49.85**	71.65	54.78	**50.68**	85.65	88.59	**87.65**
40x	M	53.05	47.11	**48.82**	76.64	59.32	**59.31**	66.87	89.97	**76.54**
	T	80.86	46.09	**53.40**	71.32	60.32	**58.98**	69.87	82.55	**74.44**
Average		**80.01**	**51.61**	**59.43**	**78.65**	**63.08**	**63.84**	**84.35**	**85.25**	**80.72**

M = Homogenous images, T = Heterogeneous images

Analysis of Table V reveals that MOSEG performs better than others and is robust against changes in magnification or image type. Except for heterogeneous images of 5x magnification factor, where improvement is small, MOSEG shows superior classification results. Furthermore, results reveal that 10x magnification factor is most suitable to image analysis as at this level, image contains enough tissue content, needed for segmentation. Our scheme depicts same phenomenon, having highest accuracy of 88.98% and 87.65% for homogenous and heterogeneous images of 10x magnification factor.

IV. CONCLUSION

The primary focus of our work was the development of new technique for segmentation of colon biopsy images and comparing it with traditionally accepted and used techniques. We proposed a new technique for detection of elliptical and nearly elliptical primitives in colon biopsy images. Proposed technique finds elliptic primitives in four angular directions, and makes use of the spatial distribution and geometric size of the primitives for defining uniformity measures in order to segment image into regions. The proposed algorithm has promising results in term of primitive detection and image segmentation, and can be extendable in future for classification of colon biopsies. In addition, GA has been employed that automatically finds optimal values for various system parameters. Thus, it makes the system totally independent of changing microscopic magnification factor and image type.

REFERENCES

[1]   M.   Fox,   http://www.livestrong.com/article/162178-stages-of-colon-adenocarcinoma/ , Updated on: Jul 1, 2010.

[2]   D. Myers, Colon cancer stages: Basics of each colon cancer stage, http://coloncancer.about.com/od/stagesandsurvivalrate1/a/ColonCancerStag.htm, Updated on: April 18, 2008.

[3]   G. D. Thomas, M. F. Dixon, N. C. Smeeton, and N. S. Williams, "Observer variation in the histological grading of rectal carcinoma," Journal of Clinical Pathology, vol. 36, no. 04, pp. 385-391, 1983.

[4]   A.Andrion et. al., "Malignant mesothelioma of the pleura: inter observer variability," Journal of Clinical Pathology, 48 pp. 856-860, 1995.

[5]   K. Masood, and N. Rajpoot, "Texture based classification of hyperspectral colon biopsy samples using CLBP," IEEE International Symposium on Biomedical Imaging, pp. 1011-1014, 2009.

[6]   K. Rajpoot, and N. Rajpoot, "SVM optimization for hyperspectral colon tissue cell classification," Medical Image Computing and Computer Assisted Intervention (MICCAI), Lecture Notes in Computer Science 3217, pp. 829-837, 2004.

[7]   K. M. Rajpoot, and N. M. Rajpoot, "Wavelet based segmentation of hyperspectral colon tissue imagery," pp. 38-43, INMIC, 2003.

[8]   R. J. Cassidy, J. Berger, K. Lee, M. Maggioni, and R. R. Coifman, "Analysis of hyperspectral colon tissue images using vocal synthesis models," Proceedings of 38th Asilomar Conference on Signals, Systems and Computers, pp. 1611-1615, 2004.

[9]   E. T. Venkatesh, P. Thangaraj and S. Chitra, "An improved neural approach for malignant and normal colon tissue classification from Oligonucleotide arrays," European Journal of Scientific Research, vol. 54, pp. 159-164, 2011.

[10] S. backert, M. Gelos, U. Kobalz, M. L. hanski, C. Bohm, and B. Mann, "Differential gene expression in colon carcinoma cells and tissues detected with a cDNA Array," International Journal of Cancer, vol. 82, pp. 868-874, 1999.

[11] K. Masood, N. Rajpoot, H. Qureshi, and K. Rajpoot, "Co-occurrence and morphological analysis for colon tissue biopsy classification," Proceedings 4th International Workshop on FIT, 2006.

[12] A. N. Esgiar, R. N. G. Naguib, B. S. Sharif, M. K. Bennett, and A. Murray, "Microscopic image analysis for quantitative measurement and feature identification of normal and cancerous colonic mucosa," IEEE Transactions on Information Technology in Biomedicine, vol. 02, no. 03, pp. 197-203, 1998.

[13] A. N. Esgiar, R. N. G. Naguib, B. S. Sahrif, M. K. Bennett, and A. Murray, "Fractal analysis in the detection of colonic cancer images," IEEE Transactions on Information Technology in Biomedicine, vol. 06, no. 01, pp.54-58, 2002.

[14] X. Li, M. Lei, D. Wang, and J. Lin, "Detection of colon cancer by laser induced fluorescence and raman spectroscopy," Proc. IEEE Engineering in Medicine and Biology Annual Conference, pp. 6961-6964, 2005.

[15] R. M. Cothren, M. V. Sivak, R. Manoharan, and M. S. Feld, "Detection of dysplasia at colon scopy using laser-induced fluorescence: A blinded study," Gastrointest. Endosc., vol. 44, pp. 168-176, 1996.

[16] N. N. Boustany, R. Manoharan, and M. S. Feld, "Analysis of normal and diseased colon mucsa using ultraviolet resonance raman spectroscopy," Proc. SPIE 2679, Advances Cancer and Other Disease, pp. 66-70, 1996.

[17] A. Molckovsky, L. Song, M. Shim, N. Marcon, and B. Wilson, "Diagnostic potential of near-infrared raman spectroscopy in the colon: differentiating adenomatous from hyperplastic polyps," Gastrointest. Endosc., vol. 57, pp. 396-402, 2003.

[18] T. D. Wang, J. V. Dam, Y. Wang, and M. S. Feld, "Fluorescence endoscopic imaging of human colonic adenormas," Gastrointest. Endosc., vol. 111, pp. 1182-1191, 1996.

[19] R. Manoharan, M. S. Feld, and G. Zonios, "Laser-induced fluorescence spectroscopy of colonic dysplasia: Prospect for optical histological analysis," Proc. SPIE, Biomedical Optics, pp. 417-421, 1995.

[20] T. D.Wang, Y. Wang, M. S. Feld, J. V. Dam, J. M. Crawford, and E. Preisinger,"Laser-induced fluorescence endoscopic imaging for detection of colonic dysplasia," SPIE, Biomedical Optics, 84, 1995.

[21] A. G. Todman, R. N. G. Naguib, and M. K. Bennet, "Visual characteristics of colon images," Proc. Medical Image Analysis and Understanding, pp. 161-164, 2001.

[22] A. G. Todman, R. N. G. Naguib, M. K. Bennett, "Orientational coherence metrics: classification of colon images based on human from perception," Proc. IEEE Canadian Conference on Electrical and Computer Engineering (CCECE), pp. 1379-1385, 2001.

[23] A. B. Tosun, M. Kandemir, C. Sokmensuer, and C. G. Demir, "Object-oriented texture analysis for the unsupervised segmentation of biopsy images," Journal of Pattern Recognition, vol. 42, 06, 1104-1112, 2009.

[24] A. B. Tosun, and C. G. Demir, "Graph run-length matrices for histopathological image segmentation," IEEE Transactions on Medical Imaging, vol. 30, no. 03, pp. 721-732, 2011.

[25] C. G. Demir, M. Kandemir, A. B. Tosun, and C. Sokmensuer, "Automatic segmentation of colon glands using object-graphs," Medical Image Analysis, vol. 14, no. 01, pp. 01-12, 2010.

[26] A. B. Tosun, C. Sokmensuer, and C. G. Demir, "Unsupervised tissue image segmentation through object-oriented texture," 20th International Conference on Pattern Recognition, pp. 2516-2519, 2010.

| OSEG | GRLM | MOSEG |

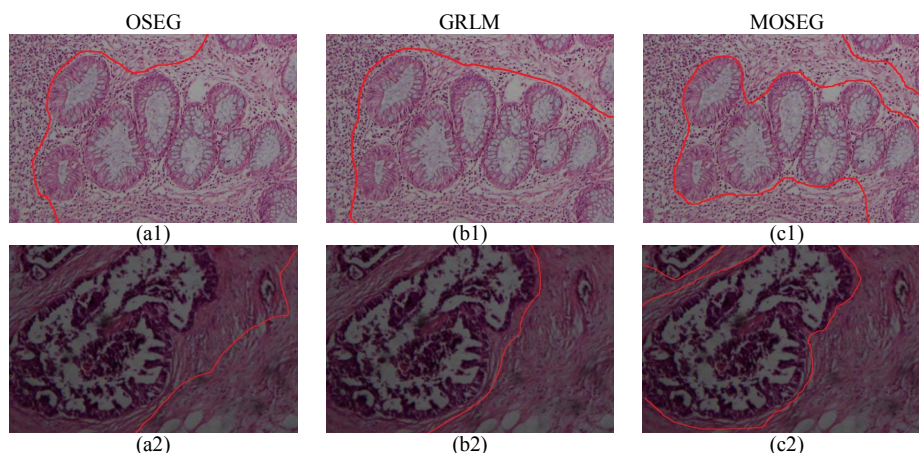| (a1) | (b1) | (c1) |

| (a2) | (b2) | (c2) |

Figure 8. Segmentation results for two images using (a1-a2) OSEG, (b1-b2) GRLM, and (c1-c2) MOSEG

139